

Massive neutral particles on heterotic string theory.

Marco Olivares*

*Instituto de Física, Pontificia Universidad de Católica de Valparaíso,
Av. Universidad 330, Curauma, Valparaíso, Chile.*

J. R. Villanueva†

*Instituto de Física y Astronomía, Universidad de Valparaíso,
Gran Bretaña 1111, Playa Ancha, Valparaíso, Chile, and
Centro de Astrofísica de Valparaíso, Gran Bretaña 1111, Playa Ancha, Valparaíso, Chile.*

(Dated: September 5, 2018)

The motion of massive particles in the background of a charged black hole in heterotic string theory, which is characterized by a parameter α , is studied in detail in this paper. Since it is possible to write this space-time in the Einstein frame, we perform a quantitative analysis of the time-like geodesics by means of the standard Lagrange procedure. Thus, we obtain and solve a set of differential equations and then we describe the orbits in terms of the elliptic \wp -Weierstraß function. Also, by making an elementary derivation developed by Cornbleet (Am. J. Phys. **61** 7, (1993) 650 - 651) we obtain the correction to the angle of advance of perihelion to first order in α , and thus, by comparing with Mercury's data we give an estimation for the value of this parameter, which yields an *heterotic solar charge* $Q_{\odot} \simeq 0.728$ [Km] = $0.493 M_{\odot}$. Therefore, in addition to the study on null geodesics performed by Fernando (Phys. Rev. D **85**, (2012) 024033), this work completes the geodesic structure for this class of space-time.

PACS numbers: 04.20.Fy, 04.20.Jb, 04.40.Nr, 04.70.Bw

Contents

I. Introduction	1
II. Time-like geodesics	2
A. The bound orbits ($E < 1$)	4
1. The circular orbits	4
2. Orbits of the first kind	4
3. Orbits of the second kind	5
4. The critical trajectories	5
B. The unbound orbits ($E \geq 1$)	7
1. Orbits of the first and second kinds	7
2. The critical trajectories	8
3. The last orbit	8
III. Perihelion precession	9
IV. Summary	10
Acknowledgments	11
References	11

I. INTRODUCTION

It is well known that an effective field theory describing string theory contains black hole solutions which have

some properties that appear different from its counterpart of the standard General Relativity [1, 2]. In this paper we will try to test those differences between both space-times by solving the complete time-like geodesics.

The starting point for studying this solutions is the effective action in heterotic string theory in four dimensions [3]

$$S = \frac{1}{16\pi} \int d^4x \sqrt{-g} \left[R - \frac{1}{12} e^{-4\Phi} H_{\mu\nu\lambda} H^{\mu\nu\lambda} - 2(\nabla\Phi)^2 - e^{-2\Phi} F_{\mu\nu} F^{\mu\nu} \right], \quad (1)$$

where Φ is the dilaton field, R is the scalar curvature, $F_{\mu\nu} = \partial_{\mu}A_{\nu} - \partial_{\nu}A_{\mu}$ is Maxwell's field strength associated with an $U(1)$ subgroup of $E_8 \times E_8$ or $\text{Spin}(32)/\mathbb{Z}_2$, and

$$H_{\mu\nu\lambda} = \partial_{\mu}B_{\nu\lambda} + \partial_{\nu}B_{\lambda\mu} + \partial_{\lambda}B_{\mu\nu} - (\Omega_3(A))_{\mu\nu\lambda}, \quad (2)$$

where $B_{\mu\nu}$ is the antisymmetric tensor gauge field, and

$$(\Omega_3(A))_{\mu\nu\lambda} = \frac{1}{4}(A_{\mu}F_{\nu\lambda} + A_{\nu}F_{\lambda\mu} + A_{\lambda}F_{\mu\nu}), \quad (3)$$

is the gauge Chern-Simons term. In this contribution we are interested in the situation when the fields $H_{\mu\nu\lambda}$ and $B_{\mu\nu}$ take the zero value, in which case action (1) reads

$$S = \frac{1}{16\pi} \int d^4x \sqrt{-g} [R - 2(\nabla\Phi)^2 - e^{-2\Phi} F_{\mu\nu} F^{\mu\nu}], \quad (4)$$

which leads to the field equations

$$\nabla_{\mu}(e^{-2\Phi} F^{\mu\nu}) = 0, \quad (5)$$

$$\nabla^2\Phi + \frac{1}{2}e^{-2\Phi} F^2 = 0, \quad (6)$$

*Electronic address: marco.olivaresrubilar@gmail.com

†Electronic address: jose.villanuevalob@uv.cl

and

$$R_{\mu\nu} = -2\nabla_\mu\Phi\nabla_\nu\Phi - 2e^{-2\Phi}F_{\mu\lambda}F_\nu^\lambda + \frac{1}{2}g_{\mu\nu}e^{-2\Phi}F^2. \quad (7)$$

Solutions to Eqs. (5, 6, 7) for a static charged black hole were found by Gibbons and Maeda [1], and independently by Garfinkle, Horowitz and Strominger [2]. So, we will refer to this black hole as the Gibbons–Maeda–Garfinkle–Horowitz–Strominger (GMGHS) black hole. Thereafter, numerous studies have been performed in the context of the heterotic string theory. For example, the solution described a black hole in four dimensions carrying mass, charge and angular momentum has been found in [3], where also the extremal limit of this solution is discussed. The same author constructed the general electrically charged, rotating black hole solution in the heterotic string theory compactified on a six-dimensional torus [4]. Also, Hassan and Sen [5] have shown that given a classical solution of the heterotic string theory which is independent of a number d of the space-times coordinates, and for which the background gauge field lies in a subgroup that commutes with p of the $U(1)$ generators of the gauge group, one can generate other classical solutions by applying an $O(d-1, 1) \otimes O(d+p-1, 1)$ transformations on the original solution. Thus, using this method, the authors constructed black string solutions in six dimensions carrying electric charge, and both, electric and magnetic type antisymmetric tensor gauge-field charge. On the other hand, the introduction of the basic aspects of string solitons, duality and black holes in string theory can be found in [6], whereas the static solutions of electrically and magnetically charged dilaton black holes with the topology of $R^2 \otimes S^{n-2}$, $R^2 \otimes S^1 \otimes S^{n-3}$ and $R^2 \otimes R^1 \otimes S^{n-3}$ constructed from the dilaton gravity theory with cosmological constant was obtained in [7].

In general relativity, the motion of particles in the background of charged black holes has been studied in various papers. For example, the motion of particles in higher dimensional charged static spherically symmetric space-times was presented in [8]. In four dimensions, the properties of the Reissner–Nordström space-time with non-zero cosmological constant was performed in [9]. Also, the motion of massless particles on this background with negative cosmological constant can be found in [10], whereas the motion of charged particles in the same space-time was made by Olivares et al. [11]. Stuchlík and Calvani [12] have studied the radial motion and perform a qualitative analysis of the allowed orbits for photons on the charged black hole with $\Lambda > 0$, whereas Pugliese et al. [13] have studied the circular motion of neutral particles on the Reissner–Nordström space-time without cosmological constant.

The study of geodesics of charged black holes in string theory is an important area of research, this is because where the gravity meets all other fundamental forces in nature and the classical equation of motion takes the form of Einstein equations plus Planck scale correction terms. A primary work by considering the circular motion and the scattering problem of charged particles by a

charged dilatonic black hole with arbitrary coupling constant a was realized by Maki and Shiraishi [14], however there is no detailed discussion of effective potential that accounts for all orbits allowed. In this work we are interested in investigating the time-like geodesics around a GMGHS black hole which corresponds to the case $a = 1$, since once this task is performed, geodesic structure for this space-time is completed, because the null geodesics were resolved fully by Fernando [15], while the study of the gravitational lensing was performed in [16]. Also, the geodesic motion of neutral test particles for equatorial time-like circular geodesic and null circular geodesic, both extremal and non-extremal case of charged black hole in string theory was studied in [17], whereas the geodesic motion in the multiply warped product space-time near the hypersurfaces in the interior of the event horizon can be found in [18].

This paper is organized as follows: in section II we presents the procedure to obtain the motion equations of massive particles in the GMGHS black hole background, and then we solve these equations to describe the allow orbits analytically. In section III we apply an elementary derivation to evaluate the perihelion precession in this space-time. Finally, in section IV we conclude with some comments and final remarks.

II. TIME-LIKE GEODESICS

With the aim to study the motion of massive neutral particles around the GMGHS black hole, we first derive the geodesic equations following the same approach given in [19–32]. Thus, we can write the GMGHS metric in the Einstein frame as [15]

$$ds^2 = -\mathcal{F} dt^2 + \frac{dr^2}{\mathcal{F}} + \mathcal{R}^2 (d\theta^2 + \sin^2\theta d\phi^2), \quad (8)$$

where the radial function, $\mathcal{R} = \mathcal{R}(r)$, is given by

$$\mathcal{R} = \sqrt{r \left(r - \frac{Q^2}{M} \right)} = \sqrt{r(r - \alpha)}, \quad \alpha \equiv \frac{Q^2}{M}, \quad (9)$$

M is the ADM mass and Q is the electric charge of the GMGHS black hole, and $\mathcal{F} = \mathcal{F}(r)$ is the well known lapse function of the Schwarzschild black hole,

$$\mathcal{F} = 1 - \frac{2M}{r} = 1 - \frac{r_+}{r}, \quad r_+ = 2M. \quad (10)$$

Also, the coordinates in (8) are defined in the ranges $0 < r < \infty$, $-\infty < t < \infty$, $0 \leq \theta < \pi$, and $0 \leq \phi < 2\pi$. So, the normalized Lagrangian associated to the metric (8) results:

$$2\mathcal{L} = -\mathcal{F} \dot{t}^2 + \frac{\dot{r}^2}{\mathcal{F}} + \mathcal{R}^2 (\dot{\theta}^2 + \sin^2\theta \dot{\phi}^2) = -1, \quad (11)$$

where $\dot{a} = da/d\tau$, and τ is an affine parameter along the geodesic that we choose as the proper time. Since

the Lagrangian (11) is independent of the cyclic coordinates (t, ϕ) , then their conjugate momenta (Π_t, Π_ϕ) are conserved and are given by

$$\mathcal{F} \dot{t} = -\sqrt{E}, \quad (12)$$

and

$$\mathcal{R}^2 \dot{\phi} = L, \quad (13)$$

in the invariant plane $\theta = \pi/2$. So, inserting Eqs. (12) and (13) into Eq. (11), we obtain

$$\left(\frac{dr}{d\tau}\right)^2 = E - V_t, \quad (14)$$

where $V_t = V_t(r)$ is the effective potential given by

$$V_t = \mathcal{F} \left(1 + \frac{L^2}{\mathcal{R}^2}\right), \quad (15)$$

which is showed in Fig. 1. From this, we can see that confined orbit can exist depending on the value of the constant of motion L . Let us start by examining the extreme condition $dV_t/dr = 0$, which leads to the cubic equation

$$r^3 - 2L_\alpha r^2 + (\alpha L_\alpha + 3L^2)r - 2\alpha L^2 = 0, \quad (16)$$

where

$$L_\alpha = \frac{L^2}{r_+} + \alpha. \quad (17)$$

So, by making the following identification:

$$r_\sigma = \frac{2L_\alpha}{3}, \quad R_\sigma = \sqrt{\frac{\chi_2}{3}}, \quad \theta_\sigma = \frac{1}{3} \arccos \sqrt{\frac{27\chi_3^2}{\chi_2^3}}, \quad (18)$$

with

$$\begin{aligned} \chi_2 &= 4 \left[\frac{4}{3} L_\alpha^2 - (\alpha L_\alpha + 3L^2) \right], \\ \chi_3 &= 4 \left[\frac{16}{27} L_\alpha^3 - \frac{2}{3} L_\alpha (\alpha L_\alpha + 3L^2) + 2\alpha L^2 \right], \end{aligned} \quad (19)$$

we can write the n th solution of Eq. (16) as a function of the angular momentum, resulting in

$$r_{ext}^{(n)}(L) = r_\sigma + R_\sigma \cos \left(\theta_\sigma + \frac{2n\pi}{3} \right), \quad (n = 0, 1, 2), \quad (20)$$

so, the stable circular orbit is obtained by setting $n = 0$ ($r_{ext}^{(0)}(L) \equiv r_s$), while the unstable circular orbit is obtained by setting $n = 2$ ($r_{ext}^{(2)}(L) \equiv r_u$). Notice that $r_s \geq r_u$, and the existence of circular orbits are linked to the value of the angular momentum. Here the equality $r_s = r_u \equiv r_l$ means that there is a critical value for L ,

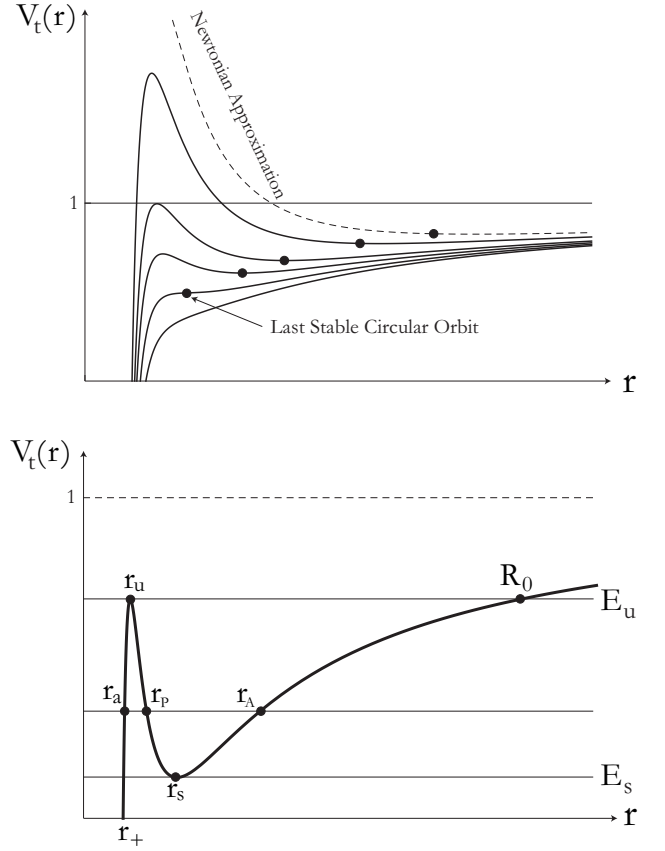


FIG. 1: Top panel: the effective potential for particles with non-vanished angular momentum. When the angular momentum takes the value L_{lsc0} , then the maximum value of the potential coincides with the minimum in a single point (point of inflection), where the black hole's last stable circular orbit (lsc0) occurs. Bottom panel: the effective potential for higher values of the critical angular momentum allows the existence of orbits confined between two turning points $r_p < r < r_a$, also for r_s stable circular orbit, and an unstable one, r_u .

say L_{lsc0} , as is referred to in the top panel of Fig. 1. So, by making the following identifications:

$$\begin{aligned} \ell_L^2 &= \frac{r_+(3r_+ - \alpha)^2}{9r_+ - \alpha}, \quad \Gamma_L^2 = \sqrt{\frac{\lambda_2}{3}} \\ \theta_L &= \frac{1}{3} \arccos \sqrt{\frac{27\lambda_3^2}{\chi_2^3}}, \end{aligned} \quad (21)$$

we can write this critical value as

$$L_{lsc0}^2 = \ell_L^2 + \Gamma_L^2 \cos \theta_L, \quad (22)$$

where

$$\lambda_2 = 324 \frac{r_+ \mathcal{R}_+^2 \ell_L^4}{(3r_+ - \alpha)^3}, \quad (23)$$

$$\lambda_3 = 108 \left[\frac{r_+^4 \mathcal{R}_+^2 (54r_+^3 - 54\alpha r_+^2 + 9\alpha^2 r_+ - \alpha^3)}{(9r_+ - \alpha)^3} \right] \quad (24)$$

$$\mathcal{R}_+ \equiv \mathcal{R}_+(r = r_+) \quad (25)$$

Therefore, at this value of the angular momentum, L_{lSCO} , the *last stable circular orbit* occurs as is shown in Fig. 1.

In addition with the principal equation of motion (14), the remaining quadratures are written as

$$\left(\frac{dr}{dt}\right)^2 = \frac{\mathcal{F}(E - V_t)}{E}, \quad (26)$$

$$\left(\frac{dr}{d\phi}\right)^2 = \frac{\mathcal{R}^4(E - V_t)}{L^2}. \quad (27)$$

First, from Eq. (15) we note that neutral massive particles with $L = 0$ have the same behavior as in the Schwarzschild space-time studied earlier, for example, by Chandrasekhar [19], Wald [34], and Schutz [35], among other authors. Therefore, we only put our attention on the motion of massive neutral particles with non-zero angular momentum. Let us consider Eq. (27), and rewrite it as

$$\left(\frac{dr}{d\phi}\right)^2 = \frac{\mathcal{R}^2}{rL^2} [-(1-E)r^3 + (\alpha(1-E) + r_+)r^2 - L_\alpha r_+ r + L^2 r_+]. \quad (28)$$

In order to obtain a full description of the motion of massive particles, we separately study the two possible cases: The bound orbits ($E < 1$) and the unbound orbits ($E = 1$).

A. The bound orbits ($E < 1$)

As is possible to see from Equation (15), $V_t \rightarrow 1$ for $r \rightarrow \infty$. This means that particles with $E < 1$ always have a turning point which corresponds to an *aphelion* distance, and depending on the value of the angular momentum, eventually has others turning point, see bottom panel of Fig. 1.

For studying the motion of particles with this characteristic, let us to rewrite Eq. (27) as

$$\left(\frac{dr}{d\phi}\right)^2 = \frac{(1-E)\mathcal{R}^2\mathcal{P}}{L^2 r}. \quad (29)$$

Here the characteristic polynomial $\mathcal{P} = \mathcal{P}(r)$ is given by

$$\mathcal{P} = -r^3 + r_b r^2 - L_\alpha (r_b - \alpha) r + L^2 (r_b - \alpha), \quad (30)$$

where

$$r_b = \frac{r_+}{1-E} + \alpha. \quad (31)$$

Therefore, depending of the nature of its roots, we shall obtain the allowed motions for this configuration.

1. The circular orbits

As we have seen, particles with $L \geq L_{lSCO}$ can stay in a circular orbit at r_{circ} ; it can be stable ($r_{circ} = r_s$) or unstable ($r_{circ} = r_u$). The periods for one complete revolution of these circular orbits, measured in proper time and coordinate time, are

$$T_\tau = 2\pi \sqrt{\frac{2r_{circ}^3 - 3r_+ r_{circ}^2 - \alpha(r_{circ}^2 - 2r_+ r_{circ})}{r_+}},$$

$$T_t = 2\pi \sqrt{\frac{2r_{circ}^3 - \alpha r_{circ}^2}{r_+}}. \quad (32)$$

On the other hand, expanding the effective potential in turn to $r = r_s$, one can write

$$V(r) = V(r_s) + V'(r_s)(r - r_s) + \frac{1}{2}V''(r_s)(r - r_s)^2 + \dots, \quad (33)$$

where $'$ means derivative with respect to radial coordinate. Obviously, in this orbits $V'(r_s) = 0$, so, by defining the *smaller* coordinate $x = r - r_s$, together with the *epicycle frequency* $\kappa^2 = 1/2V''(r_s)$, we can rewrite the above equation as

$$V(x) \approx E_s + \kappa^2 x^2 \quad (34)$$

where E_s is the energy of the particle at the stable circular orbit. Also, it is easy to see that test particles satisfy the harmonic equation of motion

$$\ddot{x} = -\kappa^2 x. \quad (35)$$

In our case, the epicycle frequency is given by

$$\kappa^2 = \kappa_{Schw}^2 \left(\frac{1 + \epsilon_1}{1 + \epsilon_2} \right), \quad (36)$$

where κ_{Schw} is the epicycle frequency in the Schwarzschild case given by [33]

$$\kappa_{Schw}^2 = \frac{r_+}{r_s^3} \left(\frac{r_s - 3r_+}{2r_s - 3r_+} \right), \quad (37)$$

and the functions that appears here are given by

$$\epsilon_1 = \frac{\alpha r_+ (2r_s - 3r_+)}{r_s (r_s - 3r_+)} \quad (38)$$

$$\epsilon_2 = \frac{\alpha r_s (5r_+ - 3r_s) + \alpha^2 (r_s - 2r_+)}{2r_s - 3r_+}. \quad (39)$$

Notice, from Eqs. (36, 38, 39), that $\kappa \rightarrow \kappa_{Schw}$ when $\alpha \rightarrow 0$.

2. Orbits of the first kind

Orbits of the first kind occur when the energy lies on the range $E_s < E < E_u$, and this case requires that

$P(r) = 0$ allows three real roots, all of which are positive; and we shall write them as

$$r_d^{(\nu)} = \frac{r_b}{3} + \sqrt{\frac{\eta_2}{3}} \cos \left[\frac{1}{3} \arccos \left(\sqrt{\frac{27\eta_3^2}{\eta_2^3}} \right) + \frac{2\pi\nu}{3} \right], \quad (40)$$

where $\nu = 0, 1, 2$, and

$$\eta_2 = 4 \left(\frac{r_b^2}{3} - L_\alpha(r_b - \alpha) \right), \quad (41)$$

$$\eta_3 = 4 \left(\frac{2r_b^3}{27} - \frac{L_\alpha \mathcal{R}_b^2}{3} + L^2(r_b - \alpha) \right), \quad (42)$$

where $\mathcal{R}_b \equiv \mathcal{R}(r = r_b)$. So, we can identify the aphelion distance as $r_d^{(0)} = r_A$, and the perihelion distance as $r_d^{(2)} = r_P$, while the third solution can be recognized as the aphelion distance to the orbits of the second kind, $r_a = r_d^{(1)}$; see bottom panel of Fig. 1. In this way, we can rewrite the characteristic polynomial (30) as

$$\mathcal{P} = (r_A - r)(r - r_P)(r - r_a). \quad (43)$$

Substituting Eq. (43) into Eq. (29) and then integrating, we obtain the polar form to the first kind orbit of the neutral massive particles, resulting

$$r(\phi) = r_A - \frac{\alpha}{4\wp(\kappa_1 \phi; g_2, g_3) - \alpha_1/3}, \quad (44)$$

where $\wp(x; g_2, g_3)$ is the \wp -Weierstraß elliptic function [36, 37], with the Weierstraß invariant given by

$$g_2 = \frac{1}{4} \left(\frac{\alpha_1^2}{3} - \beta_1 \right), \quad g_3 = \frac{1}{16} \left(\frac{\alpha_1 \beta_1}{3} - \frac{2}{27} \alpha_1^3 - \gamma_1 \right), \quad (45)$$

while the constants are given explicitly by

$$\begin{aligned} \kappa_1 &= \frac{1}{L} \sqrt{\frac{(1-E)(r_A - \alpha)(r_A - r_P)(r_A - r_a)}{\alpha}}, \\ \alpha_1 &= -\alpha \left[\frac{1}{r_A - \alpha} + \frac{1}{r_A - r_P} + \frac{1}{r_A - r_a} \right] \\ \beta_1 &= \alpha^2 \left[\frac{1}{(r_A - \alpha)(r_A - r_P)} + \frac{1}{(r_A - r_a)(r_A - \alpha)} + \frac{1}{(r_A - r_P)(r_A - r_a)} \right], \\ \gamma_1 &= -\frac{(1-E)\alpha^2}{L^2 \kappa_1^2}. \end{aligned} \quad (46)$$

In the top panel of Fig. 2 we plot the polar trajectory (44), and it shows that orbits precess between the aphelion distance, r_A , and perihelion distance, r_P . Furthermore, we can determine the angle $\chi = 2\phi_P$ corresponding to an oscillation, resulting in

$$\chi = \frac{2}{\kappa_1} \wp^{-1} \left[\frac{\alpha_1}{12} + \frac{\alpha}{4(r_A - r_P)} \right]. \quad (47)$$

In section III we will present the post-Newtonian approximation to obtain some information about the parameters of the theory.

3. Orbits of the second kind

As we have already explained, orbits of the second kind have their aphelions at r_a and eventually plunge to the radial distance $r = \alpha$. Therefore, in this case we have the following characteristic polynomial:

$$\mathcal{P} = (r_A - r)(r_P - r)(r_a - r), \quad (48)$$

so, inserting Eq. (48) into Eq. (29) and integrating, we obtain

$$r(\phi) = r_a - \frac{\alpha}{4\wp(\kappa_2 \phi; g_2, g_3) - \alpha_2/3}. \quad (49)$$

Again, $\wp(x; g_2, g_3)$ is the \wp -Weierstraß elliptic function with the Weierstraß invariants given by

$$g_2 = \frac{1}{4} \left(\frac{\alpha_2^2}{3} - \beta_2 \right), \quad g_3 = \frac{1}{16} \left(\frac{\alpha_2 \beta_2}{3} - \frac{2}{27} \alpha_2^3 - \gamma_2 \right), \quad (50)$$

where the constants are given by

$$\begin{aligned} \kappa_2 &= \frac{1}{L} \sqrt{\frac{[(1-E)(r_a - \alpha)(r_A - r_a)(r_P - r_a)]}{\alpha}} \\ \alpha_2 &= \alpha \left[\frac{1}{r_A - r_a} + \frac{1}{r_P - r_a} - \frac{1}{r_a - \alpha} \right] \\ \beta_2 &= \alpha^2 \left[\frac{1}{(r_A - r_a)(r_P - r_a)} - \frac{1}{(r_A - r_a)(r_a - \alpha)} + \frac{1}{(r_P - r_a)(r_a - \alpha)} \right] \\ \gamma_2 &= -\frac{(1-E)\alpha^2}{L^2 \kappa_2^2} \end{aligned} \quad (51)$$

The polar trajectory of the second kind is plotted in the bottom panel of Fig. 2.

4. The critical trajectories

Neutral massive particles follow critical trajectories when their energy is E_u (see bottom panel of Fig. 1), which, of course, satisfy the condition $E_u = V_t(r_u)$. Considering that the motion is performed in the region $r_u < r < R_0$, we get the characteristic polynomial as

$$\mathcal{P} = (R_0 - r)(r - r_u)^2, \quad (52)$$

and thus, the polar trajectory becomes

$$r(\phi) = R_0 - \frac{(R_0 - r_u)(R_0 - \alpha)}{(R_0 - r_u) + (r_u - \alpha) \coth^2(\omega_0 \phi)}, \quad (53)$$

where the constants are

$$R_0 \equiv r_d^{(0)}(E_u), \quad \omega_0 = \frac{\sqrt{(1-E_u)(R_0 - r_u)(r_u - \alpha)}}{2L}, \quad (54)$$

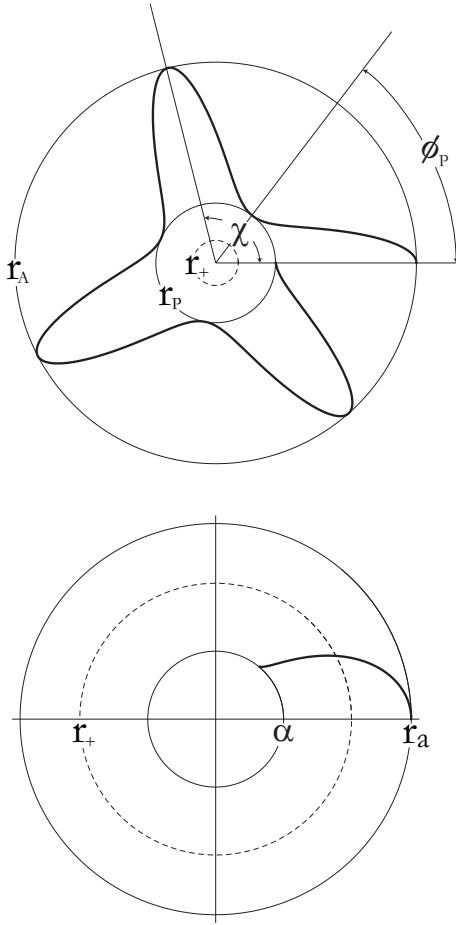


FIG. 2: Plot of the bound orbits for neutral massive particles. Top panel: Orbit of the first kind which precession between the aphelion distance, r_A , and the perihelion distance, r_P . Also, this plot shows the angle $\chi = 2\phi_P$ corresponding to an oscillation; bottom panel: orbit of the second kind for which massive particles plunge from the aphelion distance, r_a , to the interior singular surface at $r = \alpha$.

and we have plotted this motion in the top panel of Fig. 3.

On the other hand, if the motion is performed in the region $r_0 < r < r_u$, where r_0 is starting distance, then the characteristic polynomial is

$$\mathcal{P} = (R_0 - r)(r_u - r)^2, \quad (55)$$

in which case we obtain the following polar orbit

$$r(\phi) = \alpha + \frac{(R_0 - \alpha)(r_u - \alpha)}{(r_u - \alpha) + (R_0 - r_u) \coth^2(\omega_0 \phi)}. \quad (56)$$

Finally, we can obtain the polar trajectory for the last circular orbit (see top panel of Fig. 1)

$$r(\phi) = r_l - \frac{4L_{lsc0}^2 (r_l - \alpha)}{4L_{lsc0}^2 + (1 - E_l) [(r_l - \alpha) \phi]^2}. \quad (57)$$

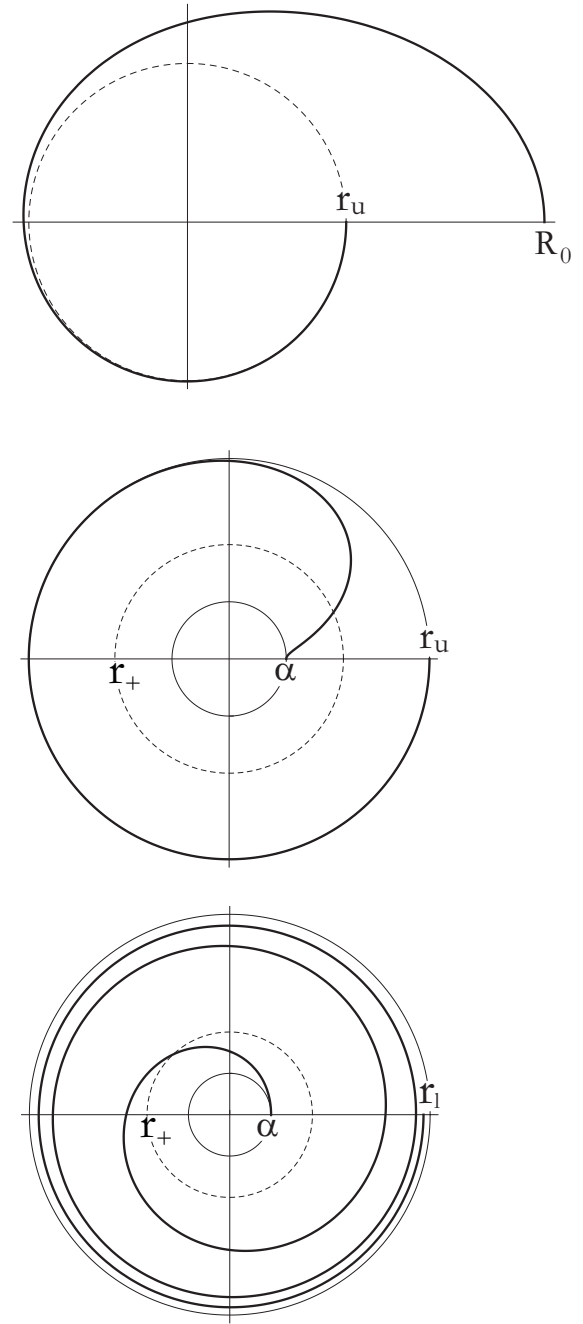


FIG. 3: Plot for critical bound orbits. Top panel: critical orbit of the first kind, whose trajectories followed by particles falling from a distance $R_0 > r_u$ and then approach asymptotically to the unstable circular orbit at r_u . Here the initial condition $r(\phi = 0) = R_0$ has been used ; middle panel: critical orbit of the second kind corresponding to the trajectories for massive particles that can go asymptotically to the unstable circular orbit at r_u or can fall into the event horizon and eventually go to the singular surface at $r = \alpha$; bottom panel: last circular orbit allowed by this space-time. The two last graphics have been made with the initial condition $r(\phi = 0) = \alpha$.

B. The unbound orbits ($E \geq 1$)

The unbound orbits are those trajectories where massive particles possess an energy $E \geq 1$. Without loss of generality, we choose the orbits with $E = 1$ for the description of this class of orbits. Therefore, the motion equation can be written as

$$\left(\frac{dr}{d\phi}\right)^2 = \frac{\mathcal{R}^2 \mathcal{B}}{(L_\alpha - \alpha)r}, \quad (58)$$

where the polynomial $\mathcal{B} = \mathcal{B}(r)$ is given by

$$\mathcal{B} = r^2 - L_\alpha r + L^2 = (r - r_1)(r - r_2). \quad (59)$$

Since the constant term in \mathcal{B} is positive, the equation $\mathcal{B} = 0$ must allow either two positive roots or a complex pair. Thus, the cases we must distinguish are those shown in Fig. 4. Provided that there are two roots and they are positive (distinct or coincident), we must continue to distinguish between orbits of two kinds: orbits of the first kind restricted to the interval, $r_2 \leq r < \infty$ (which are the analogues of the hyperbolic orbits of the Newtonian theory) and the orbits of the second kind with $r \leq r_1$ (which are, in essence, no different from the bound orbits of the second kind). When $r_1 = r_2$, the two kinds of orbits coalesce as they approach, asymptotically, a common circle from opposite sides by spiralling round it an infinite number of times. Finally, when the equation $\mathcal{B} = 0$ allows a pair of complex-conjugate roots, the resulting orbits can be considered as belonging to imaginary eccentricities.

1. Orbits of the first and second kinds

Here we study the motion of test particles by considering that two real distinct roots of the equation $\mathcal{B} = 0$ are allowed. So, recalling

$$\rho_u = \frac{1}{2} L_\alpha, \quad \text{and} \quad \Delta = \sqrt{1 - \frac{4L^2}{\rho_u^2}}, \quad (60)$$

we can write the real (positive) roots as

$$r_1 = \rho_u (1 - \Delta), \quad r_2 = \rho_u (1 + \Delta). \quad (61)$$

So, by considering the orbits of the first kind ($r > r_2$), we obtain the polar form of the trajectory in terms of the Weierstraß elliptic function, which becomes

$$r(\phi) = \frac{a_1}{3} + 4\wp\left(\frac{\phi - \Omega_0}{\sqrt{L_\alpha - \alpha}}; g_2, g_3\right), \quad (62)$$

where the Weierstraß invariants read

$$g_2 = \frac{1}{4} \left[\frac{a_1^2}{3} - b_1 \right], \quad g_3 = \frac{1}{16} \left[-\frac{a_1 b_1}{3} + \frac{2}{27} a_1^3 + c_1 \right], \quad (63)$$

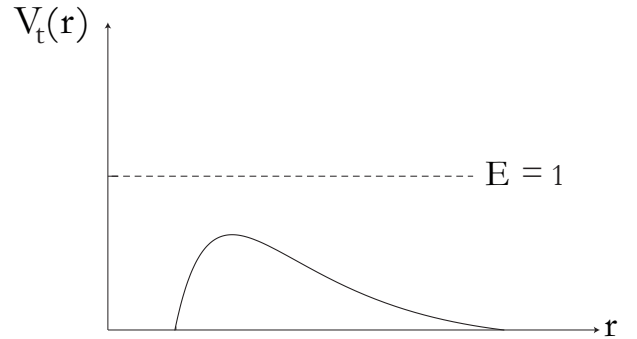
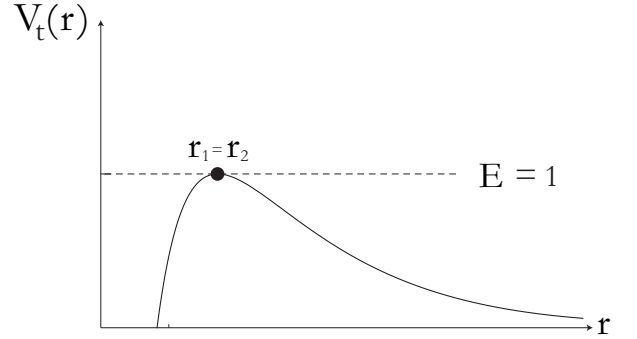
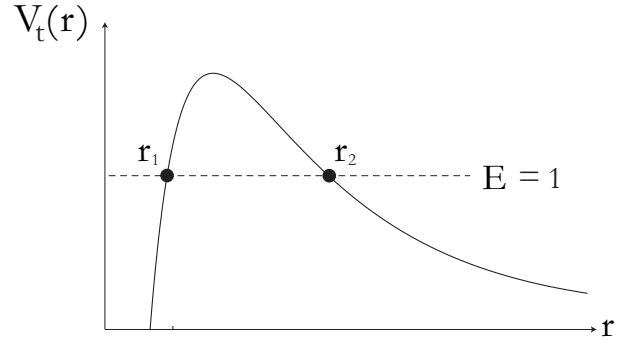


FIG. 4: The disposition of the roots of the quadratic equation $\mathcal{B} = 0$ for $E = 1$. Top panel: distinct positive roots with $r_2 > r_1$; middle panel: coincident positive roots, $r_1 = r_2 \equiv \rho_u$; bottom panel: complex roots, $r_1 = r_2^*$.

while the constants are given by

$$a_1 = L_\alpha + \alpha, \quad b_1 = \alpha L_\alpha + L^2, \quad c_1 = \alpha L^2. \quad (64)$$

Notice that in Eq. (62) we have employed the initial condition $r(0) = r_2$, which implies that

$$\Omega_0 = \wp^{-1}\left(\frac{r_2 - a_1/3}{4}; g_2, g_3\right). \quad (65)$$

From the solution (62) the deviation angle, $\varphi = 2\phi_\infty$, for this trajectory is obtained directly, and it reads

$$\varphi = 2\sqrt{L_\alpha - \alpha}\Omega_0. \quad (66)$$

In the same way, when the orbits of the second kind is taken account ($r < r_1$), we obtain the polar form of the trajectory, which is given by

$$r(\phi) = \frac{a_1}{3} + 4\wp \left(\frac{\Xi_0 - \phi}{\sqrt{L_\alpha - \alpha}}; g_2, g_3 \right), \quad (67)$$

where the initial condition $r(0) = r_1$ yields

$$\Xi_0 = \wp^{-1} \left(\frac{r_2 - a_1/3}{4}; g_2, g_3 \right), \quad (68)$$

with same set of constant (63) and (64). The orbits of the first and second kind (cf. Eqs. (62) and (67)) are plotted in Fig. 5.

2. The critical trajectories

As we have said, the neutral massive particles can fall asymptotically from a distance r_i to an unstable circular orbit at $r_1 = r_2 \equiv \rho_u$, see Fig. 4. Let us call L_u to the solution of equation $E = 1 = V_i(\rho_u, L_u)$, which is given by

$$L_u = \frac{\mathcal{R}_u}{\sqrt{s+1}}, \quad (69)$$

where $\mathcal{R}_u = \mathcal{R}(r = \rho_u)$ and $s = \rho_u/r_+$. Therefore, if $\rho_u < r_i < \infty$, then the polar trajectory is given by

$$r(\phi) = \alpha + (\rho_u - \alpha) \coth^2 \left[\frac{\sqrt{1+s^{-1}}}{2} \phi \right], \quad (70)$$

where we have used the condition $\phi = 0$ when $r \rightarrow \infty$. On the other hand, if $\alpha < r_i < \rho_u$, then the polar orbit can be written as

$$r(\phi) = \alpha + (\rho_u - \alpha) \tanh^2 \left[\frac{\sqrt{1+s^{-1}}}{2} \phi \right], \quad (71)$$

where, for simplicity, we have used the condition $\phi = 0$ when $r = \alpha$. The critical trajectories, (70) and (71), are plotted in Fig. 6.

3. The last orbit

Finally, by considering test particles with angular momentum $L_{lsc0} < L < L_u$, we can obtain the last orbit allowed in this space-time, and it correspond to the situation depicted in the right panel of Fig.4. Therefore, starting with the initial condition $\phi = 0$ at $r = \alpha$, the analytic solution to this motion is given by

$$r(\phi) = \frac{a_1}{3} + 4\wp \left(\frac{\Theta_0 + \phi}{L_\alpha - \alpha}; g_2, g_3 \right), \quad (72)$$

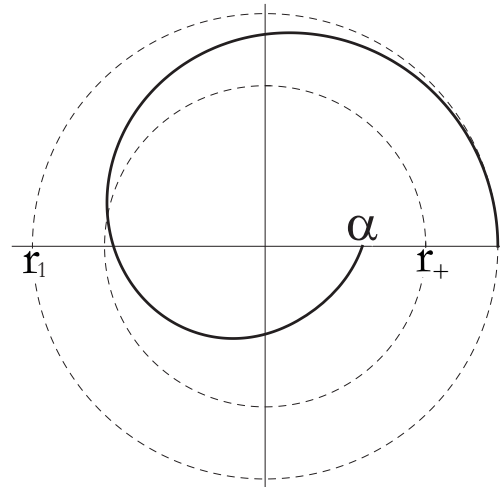
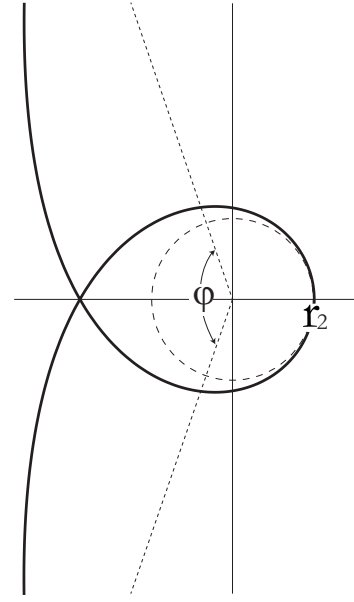


FIG. 5: The unbounded orbits with $E = 1$. Top panel: orbits of the first kind. Particles coming from the spatial infinity and approach to the minimal distance r_2 and then going again to the spatial infinity. Also, the deviation angle $\varphi = 2\phi_\infty$ is shown in this plot; bottom panel: orbit of the second kind for massive particles starting from the turning point at r_1 which cross the event horizon and arrive at the singular surface at $r = \alpha$.

where the Weierstraß invariants are given in Equation (63), and the initial condition $r(0) = \alpha$ yields

$$\Theta_0 = \wp^{-1} \left(\frac{\alpha - a_1/3}{4}; g_2, g_3 \right). \quad (73)$$

The polar trajectory given in Eq. (72) is shown in Fig. 7.

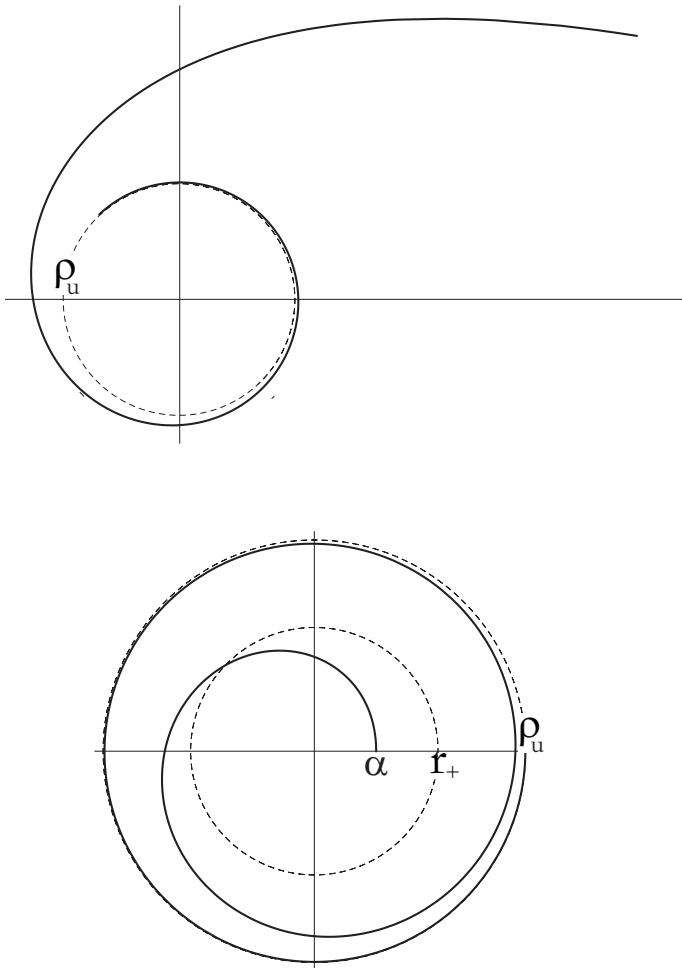


FIG. 6: The unbounded critical trajectories. Top panel: orbits of the first kind for massive particles which are coming from spatial infinity and fall asymptotically to the unstable circular orbit at ρ_u ; bottom panel: orbits of the second kind, corresponding to the trajectories followed by neutral massive particles which, depending on their initial velocity, can go either to the singular surface at $r = \alpha$ or to the unstable circular orbit at ρ_u .

III. PERIHELION PRECESSION

The following treatment, performed by Cornbleet [38], allows us to derive the formula for the advance of the perihelia of planetary orbits. The starting point is to consider the line element in unperturbed Lorentz coordinates

$$ds^2 = -dt^2 + dr^2 + r^2(d\theta^2 + \sin^2\theta d\phi^2), \quad (74)$$

together with the GMGHS line element (8). So, considering only the radial and time coordinates in the binomial approximation, the transformation gives

$$d\tilde{t} \approx \left(1 - \frac{r_+}{2r}\right) dt \quad \text{and} \quad d\tilde{r} \approx \left(1 + \frac{r_+}{2r}\right) dr. \quad (75)$$

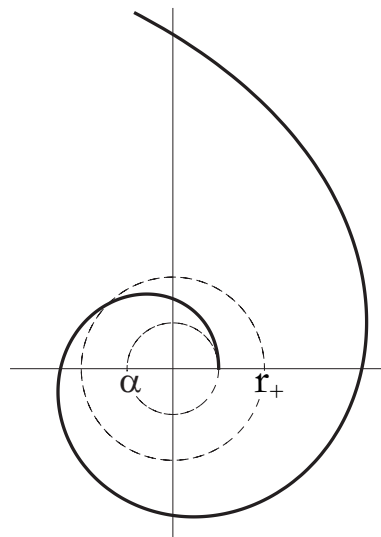


FIG. 7: The last orbit. These trajectories correspond to those followed by massive particles coming from spatial infinity which cross inexorably the event horizon and then arrive at the singular surface at $r = \alpha$.

We will consider two elliptical orbits, one the classical Kepler orbit in (r, t) space and a GMGHS orbit in an (\tilde{r}, \tilde{t}) space. Then in the Lorentz space $dA = \int_0^{\mathfrak{R}} r dr d\phi = \mathfrak{R}^2 d\phi/2$, and hence

$$\frac{dA}{dt} = \frac{1}{2} \mathfrak{R}^2 \frac{d\phi}{dt}, \quad (76)$$

which corresponds to Kepler's second law. For the GMGHS case we have

$$d\tilde{A} = \int_0^{\mathfrak{R}} \mathcal{R} d\tilde{r} d\phi, \quad (77)$$

where $d\tilde{r}$ is given by Eq. (75), and the binomial approximation for the radial function (9) is

$$\mathcal{R} \approx r \left(1 - \frac{\alpha}{2r}\right). \quad (78)$$

So, we can write (77) as

$$\begin{aligned} d\tilde{A} &= \int_0^{\mathfrak{R}} \left(r - \frac{\alpha}{2}\right) \left(1 - \frac{r_+}{2r}\right) dr d\phi \\ &\approx \frac{\mathfrak{R}^2}{2} \left(1 + \frac{r_+ - \alpha}{\mathfrak{R}}\right) d\phi. \end{aligned} \quad (79)$$

Therefore, applying the binomial approximation wherever necessary, we obtain

$$\begin{aligned} \frac{d\tilde{A}}{d\tilde{t}} &= \frac{1}{2} \mathfrak{R}^2 \left(1 + \frac{r_+ - \alpha}{\mathfrak{R}}\right) \frac{d\phi}{d\tilde{t}} \\ \frac{d\tilde{A}}{dt} &= \frac{1}{2} \mathfrak{R}^2 \left(1 + \frac{r_+ - \alpha}{\mathfrak{R}}\right) \left(1 + \frac{\alpha}{2\mathfrak{R}}\right) \frac{d\phi}{dt} \\ \frac{d\tilde{A}}{dt} &= \frac{1}{2} \mathfrak{R}^2 \left[1 + \frac{3r_+}{2\mathfrak{R}} \left(1 - \frac{2\alpha}{3r_+}\right)\right] \frac{d\phi}{dt} \end{aligned} \quad (80)$$

So, using this increase to improve the elemental angle from $d\phi$ to $d\tilde{\phi}$ then for a single orbit

$$\int_0^{\Delta\tilde{\phi}} d\tilde{\phi} = \int_0^{\Delta\phi=2\pi} \left[1 + \frac{3r_+}{2\mathfrak{R}} \left(1 - \frac{2\alpha}{3r_+} \right) \right] d\phi. \quad (81)$$

The polar form of an ellipse is given by

$$\mathfrak{R} = \frac{\ell}{1 + \varepsilon \cos \phi}, \quad (82)$$

where ε is the eccentricity and ℓ is the semi-latus rectum. In this way, plugging Eq. (82) into Eq. (81), we obtain

$$\begin{aligned} \Delta\tilde{\phi} &= 2\pi + \frac{3r_+}{2\ell} \left(1 - \frac{2\alpha}{3r_+} \right) \int_0^{\Delta\phi=2\pi} (1 + \varepsilon \cos \phi) d\phi \\ &= 2\pi + \frac{3\pi r_+}{\ell} - \frac{2\pi\alpha}{\ell}. \end{aligned} \quad (83)$$

Therefore, the perihelion advance has the standard value $\Delta\phi_{GR} = 3\pi r_+/\ell$ plus (minus) the correction term coming from the string theory $\Delta\phi_{st} = -2\pi\alpha/\ell$.

TABLE I: Sources of the precession of perihelion for Mercury

Amount (arcsec/Julian century)	Cause
$\Delta\phi_{eq} = 5028.83 \pm 0.04$ [39]	General precession in longitude (precession of the equinoxes)
$\Delta\phi_{pl} = 530$ [40]	Gravitational tugs of the other planets
$\Delta\phi_{obl} = 0.0254$ [41]	Oblateness of the Sun (quadrupole moment)
$\Delta\phi_{GR} = 42.98 \pm 0.04$ [42]	General Relativity
$\Delta\phi_T = 5603.24$	Total
$\Delta\phi_{ob} = 5599.74 \pm 0.41$ [43]	Observed
$\Delta\phi_{dis} = -3.50$	Discrepancy

Aiming to explain our results, let us consider the values for Mercury given in table I and then we add together the parts contributed by the general precession in longitude, the gravitational tugs of the other planets, oblateness of the sun and the general relativity term, we can write the total advance of perihelion as

$$\Delta\phi_T = \Delta\phi_{eq} + \Delta\phi_{pl} + \Delta\phi_{obl} + \Delta\phi_{GR}, \quad (84)$$

so, by comparing with the observational value, $\Delta\phi_{obs}$, we obtain a (negative) discrepancy between both values which can be assumed as heterotic correction of the advance of perihelion, i. e., we assume that $\Delta\phi_{dis} \simeq \Delta\phi_{st}$, see Fig. 8. Therefore, we obtain the numerical value $\alpha = 0.359$ [Km] which drive us to estimate the *heterotic solar charge*, $Q_\odot \simeq 0.728$ [Km] = $0.493 M_\odot = 8.45 \times 10^{19}$ [C]. Notice that this effect is perceived by uncharged particles, since merely corresponds to an effect of curvature in space-time, in the same way that photons are deflected

by a massive body. Finally, by considering that the number of electric charges is $n_\odot = Q_\odot/e \simeq 5.27 \times 10^{38}$, where e is the fundamental charge, we obtain the *heterotic solar electric density*, resulting

$$\rho_\odot = 3.76 \times 10^{11} \left[\frac{\text{electric charges}}{\text{m}^3} \right]. \quad (85)$$

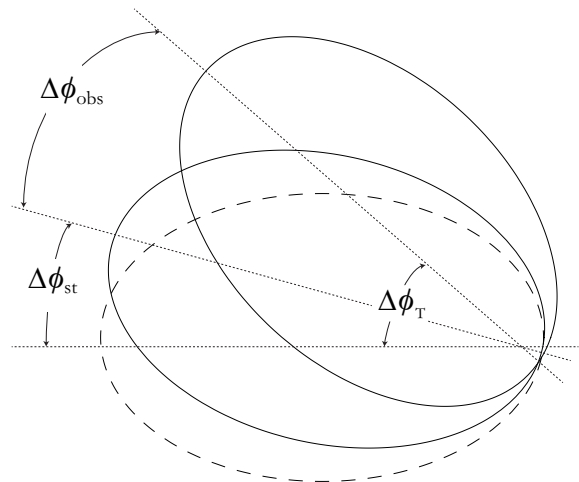


FIG. 8: The advance of perihelion. The heterotic correction gives an angle which increases the total effect, so this correction allows us to explain the discrepancy between theoretical and observational values.

IV. SUMMARY

In this paper we have studied the motion of test neutral massive particle in a Gibbons–Maeda–Garfinkle–Horowitz–Strominger (GGMHS) black hole. The equations for the geodesics in the Einstein frame were exactly solved for various values of the constants of motion of the test particles. We note that radial motion result to be equivalent to the Schwarzschild space-time, found early by other authors (for example, Chandrasekhar [19], Schutz [35], Wald [34]), so radial massive particles cannot feel any difference with the Schwarzschild counterpart. Moreover, the motion with non-zero angular momentum is different, nevertheless still presents some equivalences: there are bound and unbound orbits. For bound orbits, we studied the circular motion found the epicycle frequency, which reduces to the Schwarzschild case when $\alpha \rightarrow 0$ [33]. Also, orbits of the first and second kind are described by means of the \wp -Weierstraß elliptic function, and finally, the two class of critical trajectories, together with the last stable circular orbit, are obtained in terms of elemental functions.

On the other hand, the unbound orbits are studied for a specific value of the energy $E = 1$ since there are no change in the physics when the case $E > 1$ is considered. Thus, again the polar form of orbits of the first and

second kind was obtained in terms of the \wp -Weierstraß elliptic function, while the critical orbits were obtained in terms of elemental functions. In order to complete the geodesic structure of the GMGHS space-time, we obtain the last trajectory that fall into the horizon which also is obtained in terms of the \wp -Weierstraß elliptic function.

Additionally, we use a method developed by Cornbleet [38] to obtain the correction to the advance of the perihelion in this space-time which, by comparing with the available Mercury's data, allows us to estimate the *heterotic solar charge*, resulting $Q_{\odot} \simeq 0.728$ [Km] = $0.493 M_{\odot}$.

Finally, in addition with the work on null geodesics developed by Fernando [15], this contribution completes the full geodesic structure of the GMGHS space-time.

Acknowledgments

The authors thank to Nikolaus & Katia Vogt, Michel Curé and Radostin Kurtev for valuable helps. MO thanks to PUCV and DFA-UV. JRV is supported by FONDECYT grant N° 11130695.

-
- [1] Gibbons G. W. and Maeda K.: Black holes and membranes in higher dimensional theories with dilaton fields. Nucl. Phys. B **298**, 741 (1988).
- [2] Garfinkle D., Horowitz G. T. and Strominger A.: Charged black holes in string theory. Phys. Rev. D **43**, 3140 (1991).
- [3] Sen A.: Rotating Charged Black Hole Solution in Heterotic String Theory. Phys. Rev. Lett. **69**, 7 (1992) [arXiv: 9204046].
- [4] Sen A.: Black Hole Solutions in Heterotic String Theory on a Torus. Nucl. Phys. B **440**, 421-440 (1995) [arXiv: 9411187].
- [5] Hassan S. F. and Sen A.: Twisting Classical Solutions in Heterotic String Theory. Nucl. Phys. B **375**, 103-118 (1992) [arXiv: 9109038].
- [6] Khuri R. R.; Solitons, Black Holes and Duality in String Theory. Nucl. Phys. B (Proc. Suppl.) **61 A**, 99-110 (1998) [arXiv: 9704110].
- [7] Gao C. J. and Zhang S. N.: Topological Black Holes in Dilaton Gravity Theory. Phys. Lett. B **612**, 127-136 (2005).
- [8] Hackmann E., Kagramanova V., Kunz J. and Lämmerzahl C.: Analytic solutions of the geodesic equation in higher dimensional static spherically symmetric space-times. Phys. Rev. D **78**, 124018 (2008) [arXiv:0812.2428].
- [9] Stuchlík Z. and Hledík S.: Properties of the Reissner-Nordström space-times with a nonzero cosmological constant. Acta Phys. Slov. **52**, 363 (2002) [arXiv: 0803.2685].
- [10] Villanueva J. R., Saavedra J., Olivares M. and Cruz N.: Photons motion in charged Anti-de Sitter black holes. Astrophys. Space Sci. **344**, 437-446 (2013).
- [11] Olivares M., Saavedra J., Leiva C. and Villanueva J.R.: Motion of charged particles on the Reissner-Nordström (Anti)-de Sitter black hole Space-time. Mod. Phys. Lett. A **26**, 2923 (2011). [arXiv: 1101.0748]
- [12] Stuchlík S. and Calvani M.: Null Geodesics in black hole metrics with non-zero cosmological constant. Gen. Rel. Grav. **23**, 507 (1991).
- [13] Pugliese D., Quevedo H. and Ruffini R.: Circular motion of neutral test particles in Reissner-Nordström space-time. Phys. Rev. D **83**, 024021 (2011) [arXiv: 1012.5411].
- [14] Maki T. and Shiraiishi K.: Motion of test particles around a charged dilatonic black hole. Class. Quantum Grav. **11**, 227 (1994).
- [15] Fernando S.: Null Geodesics of Charged Black Holes in String Theory. Phys. Rev. D **85**, 024033 (2012) [arXiv: 1109.0254].
- [16] Bhadra A.: Gravitational lensing by a charged black hole of string theory. Phys. Rev. D **67**, 103009 (2003) [arXiv: 0306016].
- [17] Pradhan P. P.: ISCOs in Extremal Gibbons-Maeda-Garfinkle-Horowitz-Strominger Black holes. (2012) [arXiv: 1210.0221].
- [18] Choi J., Kim Y. and Park Y.: The geodesic motion near hypersurfaces in the warped products space-time. (2013) [arXiv: 1306.3020].
- [19] Chandrasekhar S.: The Mathematical Theory of Black Holes. Oxford University Press, New York (1983).
- [20] Cruz N., Olivares M. and Villanueva J. R.: The geodesic structure of the Schwarzschild anti-de Sitter Black Hole. Class. Quantum Grav. **22**, 1167-1190 (2005) [arXiv: 0408016].
- [21] Olivares M., Rojas G., Vásquez Y. and Villanueva J. R.: Particles motion on topological Lifshitz black holes in 3+1 dimensions. Astrophys. Space Sci. **347**, 83-89 (2013) [arXiv: 1304.4297].
- [22] Villanueva J. R. and Olivares M.: On the null trajectories in conformal Weyl gravity. JCAP **1306**, 040 (2013) [arXiv: 1305.3922].
- [23] Cruz N., Olivares M. and Villanueva J. R.: Geodesic Structure of the Lifshitz black hole in 2+1 dimensions, Eur. Phys. J. C **73**, 2485 (2013) [arXiv: 1305.2133].
- [24] Villanueva J. R. and Vásquez Y.: About the coordinate time for photons in Lifshitz space-times. Eur. Phys. J. C **73**, 2587 (2013) [arXiv: 1309.4417].
- [25] Kagramanova V., Kunz J. and Lämmerzahl C.: Orbits in the field of a gravitating magnetic monopole. Gen. Rel. Grav. **40**, 1249 (2008) [arXiv: 0708.1747].
- [26] Hackmann E., Kagramanova V., Kunz J. and Lämmerzahl C.: Analytic solutions of the geodesic equation in axially symmetric space-times. EPL **88**, 30008 (2009) [arXiv: 0911.1634].
- [27] Hackmann E., Hartmann B., Lämmerzahl C. and Sirimachan P.: The complete set of solutions of the geodesic equations in the space-time of a Schwarzschild black hole pierced by a cosmic string. Phys. Rev. D **81**, 064016 (2010) [arXiv: 0912.2327].
- [28] Hartmann B. and Sirimachan P.: Geodesic motion in the space-time of a cosmic string. JHEP **1008**, 110 (2010) [arXiv: 1007.0863].
- [29] Chen J. and Wang Y.: Timelike Geodesic Motion in Hořava-Lifshitz Spacetime. Int. J. Mod. Phys. A **25**, 1439

- (2010) [arXiv: 0905.2786].
- [30] Zhou S., Chen J. and Wang Y.: Geodesic Structure of Test Particle in Bardeen Spacetime. *Int. J. Mod. Phys. D* **21** 9, 1250077 (2012) [arXiv: 1112.5909].
- [31] Sultana J., Kazanas D. and Said J. L.: Conformal Weyl Gravity and perihelion precession. *Phys. Rev. D* **86**, 084008 (2012).
- [32] Halilsoy M., Gurtug O. and Habib Mazharimousavi S.: Rindler modified Schwarzschild geodesics. *Gen. Rel. Grav.* **45** 11, 2363 (2013).
- [33] Ramos-Caro J, Pedraza J. and Letelier P.: Motion around a Monopole + Ring system: I. Stability of Equatorial Circular Orbits vs Regularity of Three-dimensional Motion. *MNRAS* **414**, 3105-3116 (2011) [arXiv: 1103.4616]
- [34] Wald R.M.: *General relativity*. The University Chicago Press, Chicago (1984).
- [35] Schutz B.: *A First Course in General Relativity*. Cambridge University Press, New York (2009).
- [36] Weierstraß K.: Zur Theorie der Abelschen Functionen. *Crelle's J. Math.* **47** 289 (1854).
- [37] Hancock H.: *Elliptic Integrals*. John Wiley & Sons, New York (1917).
- [38] Cornbleet S.: Elementary derivation of the advance of the perihelion of a planetary orbit. *Am. J. Phys.* **61** (7), 650 - 651 (1993).
- [39] NASA Jet Propulsion Laboratory, <http://ssd.jpl.nasa.gov/?constants>
- [40] Matzner R. A.: *Dictionary of geophysics, astrophysics, and astronomy*, CRC Press. p. 356. ISBN 0849328918 (2001).
- [41] Iorio L.: On the possibility of measuring the solar oblateness and some relativistic effects from planetary ranging. *Astron. Astrophys.* **433**, 385 (2005) [arXiv:0406041].
- [42] Kraniotis G. V. and Whitehouse S. B.: Compact calculation of the Perihelion Precession of Mercury in General Relativity, the Cosmological Constant and Jacobi's Inversion problem. *Class. Quantum Grav.* **20**, 4817-4835 (2003) [arXiv: 0305181].
- [43] Clemence, G. M.: The Relativity Effect in Planetary Motions. *Rev. Mod. Phys.* **19** 4, 361-364 (1947).